

The surface compositions of Pluto and Charon



D.P. Cruikshank^{a,*}, W.M. Grundy^b, F.E. DeMeo^c, M.W. Buie^d, R.P. Binzel^e, D.E. Jennings^f, C.B. Olkin^d, J.W. Parker^d, D.C. Reuter^f, J.R. Spencer^d, S.A. Stern^d, L.A. Young^d, H.A. Weaver^g

^a NASA Ames Research Center, Moffett Field, CA 94035, United States

^b Lowell Observatory, Flagstaff, AZ 86001, United States

^c Harvard-Smithsonian Center for Astrophysics, Cambridge, MA 02138, United States

^d Southwest Research Institute, Boulder, CO 80302, United States

^e Massachusetts Institute of Technology, Cambridge, MA 02139, United States

^f NASA Goddard Spaceflight Center, Greenbelt, MD 20771, United States

^g Applied Physics Laboratory, Johns Hopkins University, Laurel, MD 20723, United States

ARTICLE INFO

Article history:

Received 6 January 2014

Revised 15 May 2014

Accepted 16 May 2014

Available online 6 June 2014

Keywords:

Pluto, surface

Charon

Spectroscopy

Satellites, composition

ABSTRACT

The surface of Pluto as it is understood on the eve of the encounter of the *New Horizons* spacecraft (mid-2015) consists of a spatially heterogeneous mix of solid N₂, CH₄, CO, C₂H₆, and an additional component that imparts color, and may not be an ice. The known molecular ices are detected by near-infrared spectroscopy. The N₂ ice occurs in the hexagonal crystalline β-phase, stable at $T > 35.6$ K. Spectroscopic evidence for wavelength shifts in the CH₄ bands attests to the complex mixing of CH₄ and N₂ in the solid state, in accordance with the phase diagram for N₂ + CH₄. Spectra obtained at several aspects of Pluto's surface as the planet rotates over its 6.4-day period show variability in the distribution of CH₄ and N₂ ices, with stronger CH₄ absorption bands associated with regions of higher albedo, in correlation with the visible rotational light curve. CO and N₂ ice absorptions are also strongly modulated by the rotation period; the bands are strongest on the anti-Charon hemisphere of Pluto. Longer term changes in the strengths of Pluto's absorption bands occur as the viewing geometry changes on seasonal time-scales, although a complete cycle has not been observed. The non-ice component of Pluto's surface may be a relatively refractory material produced by the UV and cosmic-ray irradiation of the surface ices and gases in the atmosphere, although UV does not generally penetrate the atmospheric CH₄ to interact with the surface. Laboratory simulations indicate that a rich chemistry ensues by the irradiation of mixtures of the ices known to occur on Pluto, but specific compounds have not yet been identified in spectra of the planet. Charon's surface is characterized by spectral bands of crystalline H₂O ice, and a band attributed to one or more hydrates of NH₃. Amorphous H₂O ice may also be present; the balance between the amorphization and crystallization processes on Charon remains to be clarified. The albedo of Charon and its generally spatially uniform neutral color indicate that a component, not yet identified, is mixed in some way with the H₂O and NH₃·nH₂O ices. Among the many known small bodies in the transneptunian region, several share characteristics with Pluto and Charon, including the presence of CH₄, N₂, C₂H₆, H₂O ices, as well as components that yield a wide variety of surface albedo and color. The *New Horizons* investigation of the Pluto–Charon system will generate new insight into the physical properties of the broader transneptunian population, and eventually to the corresponding bodies expected in the numerous planetary systems currently being discovered elsewhere in the Galaxy.

Published by Elsevier Inc.

1. Introduction

This paper is a review of our knowledge of the surface compositions of Pluto and its satellites on the eve of the mid-2015

* Corresponding author. Address: MS 245-6, NASA Ames Research Center, Moffett Field, CA 94035, United States.

E-mail address: Dale.P.Cruikshank@nasa.gov (D.P. Cruikshank).

encounter of the Pluto system by NASA's *New Horizons* spacecraft. We concentrate on the information that has emerged since the subject was last reviewed (e.g., Buie et al., 1997; Cruikshank et al., 1997; Marcialis, 1997; McKinnon et al., 1997; Cruikshank et al., 2005). In many respects, Pluto and Triton share the same or closely similar physical characteristics. Triton was explored in 1989, during the brief flyby of Voyager 2 through the Neptune system, revealing the atmosphere and geological activity, and

confirming the presence of N₂ ice on the surface by determining the mean molecular mass of the atmosphere. It is therefore both convenient and appropriate to compare and contrast these bodies as we review the current knowledge of Pluto.

2. Pluto

2.1. Nitrogen and methane

The first milestone in the elucidation of Pluto's composition was the identification of frozen methane on the surface. This result was based on a photometric signature in the near-infrared (Cruikshank et al., 1976) from measurements designed to distinguish H₂O, NH₃, or CH₄ in the solid state by means of their strong absorption bands in the region 1.0–2.0 μm. The identification of solid CH₄ was confirmed by spectra 4 years later (Cruikshank and Silvggio, 1980; Soifer et al., 1980). The subsequent detection of condensed N₂ on Triton (Cruikshank et al., 1984, 1988, 1993) alerted investigators to the possibility of solid N₂ on Pluto, and Pluto's nitrogen ice was discovered spectroscopically by Owen et al. (1993), via the 2-0 overtone absorption band at 2.15 μm.

The 2-0 band in N₂ absorbs light relatively weakly, having a Lambert absorption coefficient of only about 0.015 cm⁻¹ at the band center (Grundy et al., 1993). For such a weak band to be visible in the Owen et al. spectrum of Pluto, prior to escaping from the surface, the light reflected from Pluto's surface must, on average, have passed through a substantial path length within N₂ ice, of the order of multiple centimeters, as in the case of Triton. This path length is considerably greater than the millimeter path lengths in pure CH₄ ice that would explain the numerous CH₄ absorptions in Pluto's near-infrared spectrum. This discovery, which is also directly relevant to the appearance of N₂ on Triton (Cruikshank et al., 1984), changed a prevalent perception of Pluto's surface in which CH₄ is the most abundant ice to one in which CH₄ and CO (see next section) are minority contaminants in a surface dominated by N₂ ice, as for Triton.

This discovery, which is also directly relevant to the appearance of N₂ on Triton (Cruikshank et al., 1984), changed a prevalent perception of Pluto's surface and atmosphere in which CH₄ is the most abundant volatile to one in which CH₄ and CO (see next section) are minority contaminants in a system dominated by N₂, as for Triton. This realization has a profound impact on our understanding of basic properties that govern the surface–atmosphere system, not the least of which is the atmospheric pressure.

Laboratory studies of N₂ ice have shown that the shape of the 2.15-μm 2-0 absorption band depends on temperature (Grundy et al., 1993; Tryka et al., 1993, 1995), becoming narrower at lower temperatures and, at temperatures below about 41 K, developing a side-band or shoulder at around 2.16 μm. Below 35.6 K, N₂ ice undergoes a solid–solid phase transition, reorganizing its crystal structure from the hexagonal beta phase stable at higher temperatures to a cubic, lower-temperature alpha phase (Scott, 1976). The absorption spectrum changes dramatically between β- and α-N₂ (Grundy et al., 1993; Tryka et al., 1993, 1995), with the relatively broad and shallow β-N₂ absorption band being replaced by a much narrower and deeper feature in α-N₂. Spectra of Pluto are consistent with the higher temperature β-N₂ absorption, and they show the shoulder at 2.16 μm, implying an N₂ ice temperature between 35.6 and about 41 K (although caution is advisable owing to the possible undercorrection of the Pluto data for the hydrogen Brackett gamma line that appears in the solar spectrum at about the same wavelength as the shoulder). Tryka et al. (1994) made use of the temperature-dependent change in breadth of the 2.15-μm band to solve for an N₂ ice temperature, obtaining 40 ± 2 K. But again, caution is advisable, since band

widths are influenced by scattering effects as well as temperature effects, and with only one absorption band to work with, Tryka et al. had to assume the scattering characteristics of the surface, rather than being able to solve for them. Quirico and Schmitt (1997a) reported no effect of dissolved CH₄ on the N₂ ice absorption band. Although strong effects are not expected, laboratory studies have not yet ruled out subtle influences by other potential minority contaminants on the spectral behavior of the N₂ ice absorption that could further complicate its use as a spectral thermometer.

Fig. 1 shows the spectrum of Pluto from 0.8 to 2.5 μm, with the individual absorption bands or band complexes identified.

Prokhvatilov and Lantsevich (1983) derived an equilibrium binary phase diagram for condensed N₂ and CH₄ using X-ray diffraction techniques (see Fig. 2). This phase diagram shows that N₂ and CH₄ are completely miscible in one another as liquids, but on freezing, N₂ is only partly soluble in CH₄ ice and CH₄ is only partly soluble in N₂ ice. The solid solution solubility limits for the two species in one another are functions of temperature, with greater solubilities at higher temperatures. For a plausible Pluto volatile ice temperature of 40 K, the diagram shows that in CH₄ ice, the solubility limit is about 3% N₂ (molar concentration), and in N₂ ice the solubility limit is about 5% CH₄. For any bulk composition between the solubility limits, under conditions of thermodynamic equilibrium, two phases must be present simultaneously: CH₄ and N₂, each with the other dissolved within it at the relevant solubility limit. The relative abundances of the two phases can be ascertained from the phase diagram using the lever rule. Although this point was first underscored in the planetary science literature almost 30 years ago (Lunine and Stevenson, 1985), subsequent publications have been somewhat inconsistent in recognizing that if both CH₄ and N₂ are present and in thermodynamic equilibrium, then it is impossible for either pure CH₄ or N₂ to exist. Although pure ices could potentially exist under transient disequilibrium conditions, laboratory studies have not yet been done to establish how long such a configuration could last, should it ever arise on the surface of Pluto.

A slight mismatch between the wavelengths of CH₄ bands observed in telescopic spectra of Pluto and Triton (e.g., Owen et al., 1993; Cruikshank et al., 1993) and the wavelengths of CH₄ ice absorption bands measured in the laboratory (e.g., Grundy et al., 2002) prompted a laboratory investigation of CH₄ diluted in N₂ ice (Quirico and Schmitt, 1997a). That study showed that CH₄ absorption bands shift to shorter wavelengths when the CH₄ is diluted in N₂ ice, leading to more than a decade of work in which Pluto's spectrum was interpreted in terms of a combination of “diluted” and “pure” CH₄ components (e.g., Douté et al., 1999; Tegler et al., 2010, 2012). Clearly, neither component alone could match Pluto's CH₄ bands, and the inclusion of both resulted in considerably better fits (Douté et al., 1999). This approach made use of the available laboratory spectra at the time, specifically pure CH₄ (Grundy et al., 2002) and CH₄ highly diluted in N₂ ice (Quirico and Schmitt, 1997a). But thermodynamically, pure CH₄ ice is inconsistent with the presence of N₂ in an equilibrated system. The problem was that laboratory data were simply not available for the two components called for by the phase diagram: CH₄ saturated in N₂ ice and N₂ saturated in CH₄ ice. Brunetto et al. (2008) began to explore compositions outside the solubility limits, but their experiments were of limited use to modelers, since their samples consisted of combinations of the two intergrown phases with unspecified textures. The two phases at their solubility limits were finally studied separately in the laboratory during 2011–2013, but have not yet been used in a systematic analysis of Pluto spectra (Protospapa et al., 2013).

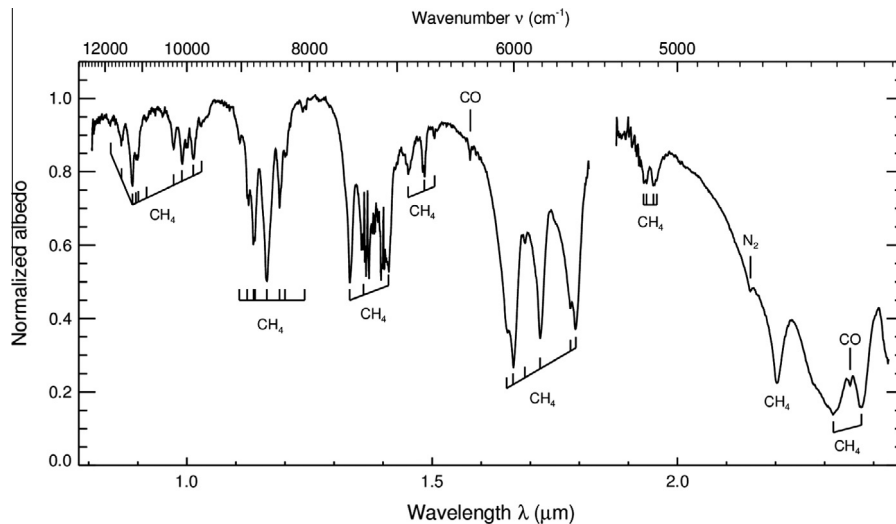


Fig. 1. Average of the best spectra of Pluto (including the light from Charon) from 65 data sets obtained from 2001 to 2013 in a monitoring program (Grundy et al., 2013). Reproduced courtesy Elsevier.

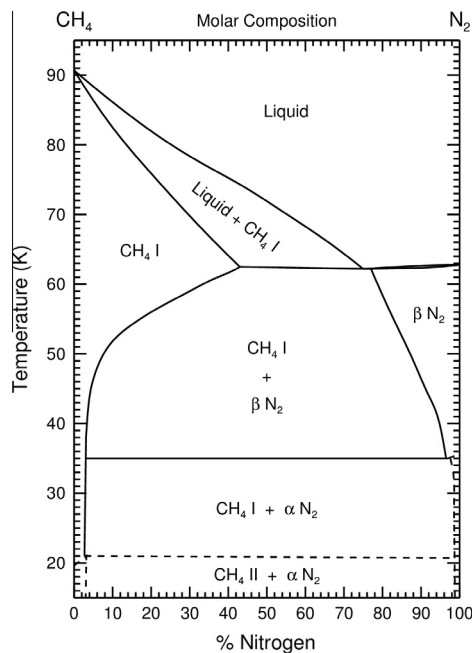


Fig. 2. Binary phase diagram of $N_2 + CH_4$ by Prokhvatilov and Lantsevich (1983). From Tegler et al. (2012), © AAS. Reproduced with permission.

2.2. Other species

Solid carbon monoxide is found on both Pluto and Triton by means of the (2-0) band at 2.352 μm and the weaker (3-0) band at 1.578 μm (Owen et al., 1993; Douté et al., 1999). Protospapa et al. (2008) found convincing evidence for the CO fundamental at 4.67 μm , possibly blended with methane and some nitrile species. While CO is miscible in N_2 and their vapor pressures are similar, the matrix shift in wavelength of CO in N_2 is too small to be detected in spectra currently available (Quirico and Schmitt, 1997b). It is therefore unclear if CO primarily occurs in the N_2 matrix, or if it is a pure condensed ice or frost. Lellouch et al. (2011a) have found spectroscopic evidence for CO in Pluto's atmosphere with an estimated abundance of $CO/N_2 = 5 \times 10^{-4}$. The estimated surface abundance is 1×10^{-4} (Lellouch et al., 2011b). For

comparison, the Lellouch et al. values of CO/N_2 for Triton are 6×10^{-4} and 1×10^{-3} for the atmosphere and surface, respectively.

In addition to the normal ^{12}C bands, the ^{13}C (1-0) band appears to be present at 2.405 μm , but with a strength relative to the ^{12}C band that cannot be reconciled with plausible $^{12}\text{C}/^{13}\text{C}$ abundances (Cruikshank et al., 2006; DeMeo et al., 2010). This band is coincident with a band of solid C_2H_6 , and thus provides evidence for the presence of this hydrocarbon that is produced by the photochemistry of CH_4 . In earlier work, Nakamura et al. (2000) found that Pluto's strong bands at 2.28 and 2.32 μm are best fit with a combination of CH_4 and C_2H_6 absorption, but their 2.405- μm region is discrepant with ethane. At longer wavelengths, Sasaki et al. (2005) noted that their Pluto data were best fit when ethane was added, but they did not clearly identify ethane bands. Spectra by Verbiscer et al. (2007) support the evidence for C_2H_6 bands in the interval 2.3–2.45 μm . Merlin et al. (2010) and Cook et al. (2013) also found that models of Pluto's near-IR reflectance were improved by the addition of ethane ice. Estimates of the abundances of ethane on Triton and Pluto suggest that this ice is deposited on relatively short time-scales by precipitation from the atmosphere, where it is produced by photochemistry (e.g., Krasnopolsky and Cruikshank, 1999). Similarly, Cook et al. (2013) found that models of Pluto's reflectance in the near-IR were improved slightly by the addition of C_2H_4 (ethylene), but this molecule has not been identified by observations of unique absorption bands.

The spectrum of Pluto beyond 2.5 μm has been explored in a preliminary way by Sasaki et al. (2005), Olkin et al. (2007), and Protopapa et al. (2008), in part to search for additional molecular species, including other hydrocarbons. Fig. 3 is a composite spectrum of Pluto (without Charon light) that is plotted together with a model consisting of a geographic mixture of pure CH_4 ice with two different grain sizes, CH_4 and CO dissolved in solid N_2 , the nitrile CH_2CHCN , and titan tholin. The nitrile was included to help explain absorption in the spectrum near the CO band at 4.67 μm , but its inclusion in the model does not constitute an identification of this material.

Another photochemical product of CH_4 and N_2 is HCN (e.g., Krasnopolsky and Cruikshank, 1999), which is produced both in the gaseous and solid states. Burgdorf et al. (2010) found the 4.76- μm ν_1 stretching mode band of HCN in absorption in the spectrum of Triton. A similar band occurs at the same wavelength

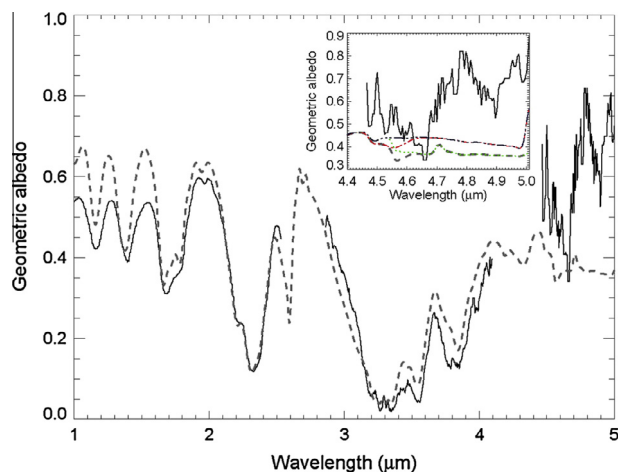


Fig. 3. Spectrum of Pluto (solid line) (not including the light from Charon), 1–5 μm , from Protopapa et al. (2008). The dashed line is a best-fitting model at the same resolution as the observational data. Gaps in the Pluto spectrum (2.5–2.85 and 4.1–4.5 μm) correspond to opaque telluric absorption intervals. Inset: Enlargement of the longest wavelength segment, with three models. Gray dashed line is the model shown for the full 1–5 μm spectral region; dotted green line is the best model with CH_3D (4.34 and 4.56 μm removed); the red line is the best model with the CO ice band at 4.67 μm removed; the dash-dot line is the best-fitting model including the nitrile CH_2CHCN only. Reproduced courtesy Astronomy and Astrophysics. (For interpretation of the references to color in this figure legend, the reader is referred to the web version of this article.)

in the spectrum of Pluto obtained by Protopapa et al. (2008), and while HCN is expected to occur in detectable amounts, this band has not yet been modeled in a mix of other components known to exist on Pluto.

2.3. Distribution of ices on Pluto

Near-infrared wavelengths between about 0.7 and 2.5 μm are especially useful for Earth-based remote monitoring of Pluto's ices. In addition to the numerous volatile ice vibrational overtone and combination modes in this wavelength range, there is ample solar flux illuminating Pluto. Also the terrestrial atmosphere is relatively transparent, and emits relatively little light. But to most Earth-based observatories, Pluto is only a point source at these wavelengths, often not even spatially resolved from its largest satellite Charon. So the only practical way to investigate the spatial distribution of Pluto's ices has been to take advantage of changing viewing geometry over time.

The most obvious way Pluto's geometry changes over time is through its 6.4-day rotation. This motion causes a persistent visible lightcurve as regions having distinct albedos rotate into and out of view. Similar 6.4-day periodicities have been reported in Pluto's near-infrared spectral features, beginning with the CH_4 bands, which were found to be weaker around the time of lightcurve minimum and stronger around the time of lightcurve maximum, indicating that CH_4 on Pluto's surface is associated with regions of higher albedo (Buie and Fink, 1987; Marcialis and Lebofsky, 1991). Additional complexities emerge when different CH_4 absorption bands are compared. The stronger CH_4 bands are well correlated with the visible lightcurve, but the weaker CH_4 bands exhibit maximum absorption at longitudes that shift toward the sub-Charon hemisphere (Grundy and Fink, 1996). The weaker the band, the larger is the longitudinal shift (Grundy and Buie, 2001). This behavior suggests that methane ice does not have the same light scattering properties in all regions where it occurs on Pluto. Relatively short mean optical path lengths through CH_4 are sufficient to produce the strong CH_4 bands, but not the weak ones.

Greater path lengths through CH_4 seem to be needed on the sub-Charon hemisphere to produce that region's appreciable absorption in the weaker CH_4 bands.

Pluto's CO and N_2 ice absorptions have fewer, and more subtle absorption bands, but a new generation of infrared grating spectrometers revealed that the absorptions of those two ices are also strongly modulated by Pluto's 6.4 day rotation, with the strongest absorption of both ices being seen when Pluto's anti-Charon hemisphere is oriented toward the observer (Grundy and Buie, 2001; Grundy et al., 2013). HST albedo maps of Pluto's surface show a bright patch centered on the anti-Charon hemisphere (Buie et al., 1992, 2010a; Stern et al., 1997), so it has been speculated that this region could be the site of the CO and N_2 absorption. Another way to detect N_2 ice is through its effect on the more readily observable CH_4 bands. As discussed in a previous section, when CH_4 is dissolved in N_2 , its absorptions shift to shorter wavelengths. Using cross-correlation to measure wavelength shifts in Pluto's CH_4 bands reveals that the shifts are greatest when Pluto's anti-Charon hemisphere is oriented toward the observer (Grundy et al., 2013). This is the same hemisphere where the N_2 ice absorption is strongest, so both methods are in accord in placing more N_2 ice there.

The consistency in these spectral changes and in the lightcurve variability from one Pluto rotation to the next argues against thick or variable cloud cover obscuring the view of the surface. It also says that the spatial distribution of Pluto's ices is static, at least on timescales of weeks to months.

Over longer timescales, the viewing geometry changes in another way. Pluto's obliquity is high. Its spin pole differs 120° from its heliocentric orbit pole, so the sub-solar latitude on Pluto varies seasonally over $\pm 60^\circ$ of latitude, a considerably wider tropic band than the current range of $\pm 23.4^\circ$ for Earth. Pluto's last equinox was on 1987 December 16, when the sub-solar latitude crossed Pluto's equator from the southern into the northern hemisphere (using the orbit from Buie et al., 2012). By the time of the 2015 *New Horizons* encounter, it will have reached 51° North, well on its way to its 60° maximum during Pluto's northern summer solstice in the late 2020s. Earth-based observers were seeing Pluto's equatorial regions during the 1980s, while more recent observations are increasingly dominated by high northern latitudes. Differences in ice composition or texture between equatorial and polar regions would show up as a gradual secular evolution of Pluto's spectral features.

The first such secular spectral change to be reported was a decrease in absorption in Pluto's weak 0.73- μm CH_4 band from the 1980s through the 1990s (Fink and DiSanti, 1988; Grundy and Fink, 1996). Grundy and Buie (2001) found that the strong CH_4 bands were progressing in the opposite direction, increasing in strength during the 1990s. That trend continued at least into the early 2000s, although it seems to have slowed in recent years (Grundy et al., 2013). That paper also reported tentative declines in Pluto's N_2 and CO absorptions during the 2000s. All of these secular spectral changes could potentially be attributed to the changing viewing geometry, if the N_2 , CO, and weak CH_4 absorption bands were predominantly formed in low-latitude regions while the strong CH_4 bands were formed at high latitudes.

But interpreting these longer-term changes in terms of a static distribution of ices is problematic because Pluto's N_2 , CO, and CH_4 ices are volatile enough to be mobile on seasonal timescales. Of the three, N_2 is the most volatile (Fray and Schmitt, 2009). Models show that in regions of Pluto receiving the most sunlight, a layer of N_2 ice of the order of a centimeter thick could sublimate into the atmosphere every Earth year (e.g., Spencer et al., 1997; Trafton et al., 1998). That sublimation is balanced by condensation in regions absorbing less sunlight, but the details depend sensitively on the spatial distribution of ices as well as the thermal inertia of the substrate, emissivity, etc. Pluto's surface atmospheric

pressure determined from stellar occultations increased between two events that were observed in 1988 and 2002 (e.g., [Elliot et al., 2003](#); [Sicardy et al., 2003](#)), but it is not known if this was a gradual change between the 2 years, or an episodic increase. The change represented roughly a doubling of the atmospheric pressure; subsequent occultations have yielded values of the pressure consistent with the 2002 point ([Olkin et al., submitted for publication](#)).

The temporal variability of Pluto's visible wavelength lightcurve and albedo features cannot be explained by the evolution of viewing geometry alone (e.g., [Schaefer et al., 2008](#); [Buie et al., 2010a](#)). The same is expected to be true for Pluto's various ice absorption bands. But without a much longer time baseline and/or spatially-resolved near-infrared spectra, it is hard to distinguish seasonally changing ice distributions from changes in sub-viewer latitude. [Grundy and Buie \(2001\)](#) suggested a possible way to separate the two effects by exploiting the parallax from Earth's motion around the Sun. This motion causes a $\pm 2^\circ$ yearly oscillation in the sub-Earth latitude on Pluto superimposed on its gradual northward progression of about 2° per Earth year during the early 2000s. Thanks to this parallax, it is possible to observe Pluto at the same sub-Earth latitude in two consecutive years. Grundy and Buie argued that observations at times with matching sub-Earth latitudes, but separated in time by a year, should only show effects of ongoing seasonal volatile transport, and not those due to the gradual changes in viewing geometry and the gradual change in the sub-solar point.

Unfortunately, expected spectral changes over only the 1 year time base offered by this technique are small, so high signal precision is critical, and since Pluto's spectrum varies so much as it spins on its axis, it is essential to match the sub-Earth longitude, too. [Grundy and Buie \(2001\)](#) were able to obtain a few geometrically-matched observation pairs during 1997–1998 and [Grundy et al. \(2013\)](#) got a few more such pairs during 2005–2006. Comparison between the matched pairs showed little change in N_2 and CO absorptions, favoring a static distribution of those ices. But they showed unexpected decreases in the strengths of the strong CH_4 bands, counter to the secular trend. One possible explanation is that seasonal volatile transport is diminishing the CH_4 absorptions, but this effect is masked by an even greater increase caused by the northern polar regions rotating into view. In their latest update, [Grundy et al. \(2014\)](#) report on an accelerating decrease in CO and N_2 absorption in the last few years, something that cannot be explained with a static distribution of N_2 and CO ices. They also note that changes in observed absorption bands need not be strictly related to the projected area covered by each ice. Changes in ice texture could also lead to spectral changes. They argue that the decline in N_2 and CO absorption, as well as a decline in the shifts of the CH_4 bands might be caused by sublimation of small amounts of N_2 from an N_2 -dominated $N_2:CH_4$ solid solution saturated with CH_4 . Removing N_2 would require exsolution of CH_4 to keep the composition from exceeding the solubility limit, and if that leads to formation or growth of small CH_4 crystals, they could increase scattering and decrease the mean optical path length in the N_2 ice.

Short-term changes on Pluto on the order of days or months have generally not been noted, although [Tholen and Buie \(1988\)](#) showed the lightcurve of the 1988 April 18 transit of Pluto by Charon in which there is evidence of a possible post-eclipse brightening effect. Temporary condensation of an atmospheric component on Pluto's surface by the cooling induced by the passage of Charon's shadow could plausibly raise the albedo of the affected region on the planet. Further examples of the lightcurve of the 1988 event have not been reported.

In a surface composed of sublimating and/or condensing volatile ices, it is natural to expect near-surface compositional

gradients to arise from the fact that N_2 , CO, and CH_4 have different volatilities. As noted by [Grundy and Fink \(1996\)](#), such a configuration could produce observable spectral consequences, since different wavelengths sample different depths on average. Weak absorption bands probe deeper within a surface than strong bands do because photons at weakly-absorbing wavelengths can pass through more material before being absorbed. Many authors have considered this possibility for Pluto and other bodies with CH_4 ice absorption bands, by comparing compositions derived for weak and strong CH_4 bands (e.g., [Licandro et al., 2006a](#); [Tegler et al., 2008](#); [Abernathy et al., 2009](#); [Merlin et al., 2009](#)). The results have been inconsistent for a number of reasons. Different papers have looked at different CH_4 absorption bands, and they have used different methods to assess compositions. Cross-correlation is a convenient way to measure a wavelength shift, but converting such a shift into a composition is far less straightforward.

Shifts for different CH_4 bands cannot be directly compared, because each band shifts by a different characteristic amount when the CH_4 is diluted in N_2 ([Quirico and Schmitt, 1997a](#)). A measured shift can be compared with the shift for the same band in highly diluted CH_4 , as tabulated by [Quirico and Schmitt \(1997a\)](#), but quantitative values for the shifts for many weaker, shorter wavelength CH_4 bands are not available in the literature. An additional complicating factor is the phase behavior of N_2 and CH_4 described earlier. As progressively more N_2 is added to CH_4 ice, there is not a simple, monotonically increasing shift. When the solubility limit is exceeded, a second, N_2 -rich phase appears, with a much larger shift. Both phases are present simultaneously, and both contribute to the observed absorption band. The CH_4 -rich component has a relatively small shift and the N_2 -rich component has a larger shift. The best approach seems to be to model both of these phases and compute the CH_4/N_2 ratio from their relative abundances, using optical constants for the two phases at their solubility limits ([Protopapa et al., 2013](#)). Using an approach like this, but with estimated rather than measured optical constants, [Tegler et al. \(2010, 2012\)](#) found no evidence of a vertical compositional gradient in the CH_4/N_2 ratio on Pluto.

2.4. Pluto in the ultraviolet

Ultraviolet spectroscopy has not yielded definitive identifications of surface components, although [Stern et al. \(2012\)](#) have reported an absorption feature between 210 and 240 nm. They note that various hydrocarbons and nitriles produce absorptions in this wavelength range, but do not make a specific identification. In earlier work, also with the Hubble Space Telescope, [Krasnopolsky \(2001a,b\)](#) found that the mean geometric albedo across the interval 200–250 nm is nearly constant at 0.22, but that overall intensity variations attributed to rotational phase and the episodic appearance of atmospheric haze occur. [Krasnopolsky's \(2001a\)](#) spectra do not reveal diagnostic surface absorption bands, but he attributes the large brightness changes in the same spectral interval as the [Stern et al. \(2012\)](#) absorption feature to the formation of strongly backscattering atmospheric haze particles in a global weather-like phenomenon. Planetary spectra in the ultraviolet region present special challenges of interpretation because of the overlap and interplay of atmospheric and surface components, the former of which can be variable on several time scales and spatial scales. In the case of Pluto, at the present time we have no clear picture of the surface compositional information contained in the ultraviolet spectral region.

2.5. Non-ice component of Pluto's surface

The ices detected spectroscopically on Pluto's surface are colorless, yet Pluto itself has a reddish color in the spectral region

0.3–1.0 μm (Bell et al., 1979; Barker et al., 1980; Buie and Fink, 1987). Photometry of the Pluto–Charon system by Reinsch et al. (1994) showed that the colors of the combined pair averaged over a full rotation are $(B-V) = 0.846 \pm 0.010$ and $(V-R) = 0.462 \pm 0.021$. The mutual events allowed a separation of the color of Pluto from that of Charon; Binzel (1988) found $(B-V) = 0.867 \pm 0.008$ for the anti-Charon-facing hemisphere and 0.700 ± 0.010 for the Charon-facing hemisphere. For the Sun, $(B-V) = 0.65$ and $(V-R) = 0.54$. Thus, Pluto is reddish in color in the B–V interval, but the Pluto–Charon pair is slightly blue in the V–R interval in these full pole-to-pole global views of the respective hemispheres of Pluto and Charon. The photometric colors are in general accord with the spectral shape from Barker et al. and Bell et al. (Fig. 4), and with the Buie and Fink (1987) spectra showing the Pluto–Charon pair to be distinctly red from 0.58 to 0.90 μm .

The (B–V) color of Pluto has the longest timebase of measurements of any color or spectroscopic information. From the interval spanning 1953–2000, the color was seen to be constant to within a few tenths of a percent. The invariability of this color is remarkable in view of the fact that the 6.4-day rotational lightcurve varies by 30% (in its equatorial view) and the sub-solar latitude changed from -57° in 1953 to $+26^\circ$ in 2000. Clearly the coloring agent is ubiquitous over the surface, including both dark and bright regions, and was not affected by any volatile transport or surface modification that might have been active over this time. This picture changed dramatically in 2002 when HST-based lightcurve observations showed a global change in color to a redder $(B-V) = 0.954$, and that color persists to the present day. One additional change is that the color is no longer constant over a rotation with a modulation between 0.92 and 0.98. A more complete discussion of these observations can be found in Buie et al. (2010b) where this change was first noted. No detailed models exist to explain these observations but are consistent with a picture where the coloring agent is mixed into the upper surface layers with a distinct unit that was deeper in the surface that has a greater abundance of red material. These data lack sufficient spatial resolution for more complex interpretations but it will be very interesting to see if the uniformity of color is only at a large scale or if it is truly fully mixed at all spatial scales. The data from the *New Horizons* encounter will provide crucial data from which to further understand the red non-ice material.

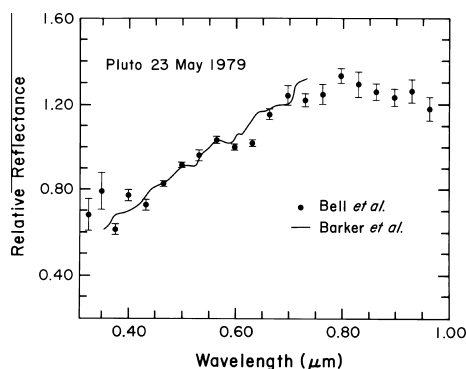


Fig. 4. Normalized spectral reflectance of the Pluto–Charon pair from two sources. The Barker et al. (1980) spectrum is derived from multiple observations in February, 1979, while the Bell et al. (1979) photometry was obtained with a set of discrete filters. Other spectra by Buie and Fink (1987) in April, 1983, show that from 0.58 to 0.90 μm the spectrum of the pair is reddish (apart from discrete CH_4 absorption bands). The Bell et al. (1979) data were first published in the review by Cruikshank et al. (1997). From *Pluto and Charon* edited by S. A. Stern and D. J. Tholen © 1997 The Arizona Board of Regents. Reprinted by permission of the University of Arizona Press.

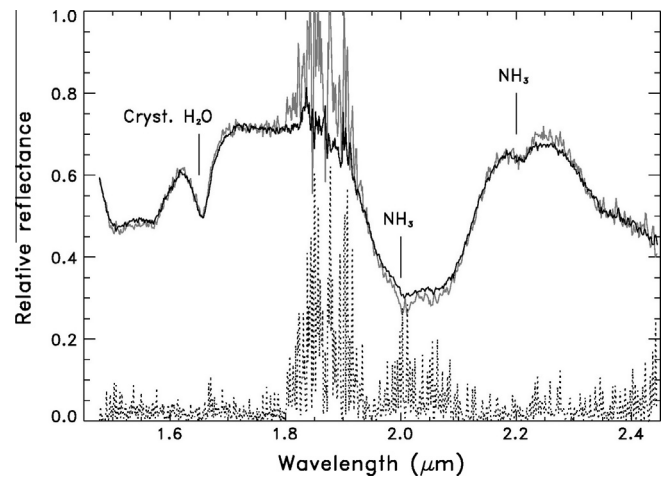


Fig. 5. Two spectra of Charon showing H_2O ice bands, including the 1.65- μm diagnostic band of hexagonal crystalline H_2O ice. NH_3 hydrate bands are shown at 2.0 and 2.21 μm . Dotted lines represent the difference between the two individual spectra of Charon, and are small (within 5–10%, except in the region of the telluric atmospheric absorption (~ 1.8 –2.1 μm)). The gray line was for a Charon sub-Earth longitude of 242° and the black line was 188° . The anti-Pluto hemisphere is 180° . From Merlin et al. (2010). Courtesy Elsevier.

The red component of Pluto's surface is generally attributed to some non-ice material, possibly the relatively refractory product of the irradiation of the ices by solar ultraviolet light and/or galactic cosmic rays. The solar UV flux that includes UV-A, UV-B, and UV-C (100–400 nm) at Pluto's mean heliocentric distance (39.3 AU) is $5.63 \times 10^{13} \text{ eV cm}^{-2} \text{ s}^{-1}$, while the cosmic ray flux deposits $6.9 \times 10^9 \text{ eV cm}^{-2} \text{ s}^{-1}$ and the solar wind (e^- , H^+ , He^+) energy flux is 2.6×10^8 (Madey et al., 2002). Thus, the UV energy flux at Pluto's distance greatly exceeds the cosmic ray flux, but the tenuous atmosphere is opaque to UV throughout most of Pluto's presumed seasonal atmospheric density cycle, and therefore the principal energy source for processing the surface materials is expected to be cosmic rays, with a small possible contribution by charged particles in the solar wind. Ultraviolet processing of Pluto's atmospheric components produces other molecules that precipitate to the surface, including C_2H_2 , C_4H_2 , HC_3N , HCN , and C_2H_6 , which in their monomolecular forms are also colorless (e.g., Krasnopolsky and Cruikshank, 1999).

Laboratory studies of the irradiation of ice mixtures relevant to Pluto with both UV and charged particles have been described by Bohn et al. (1994), Moore and Hudson (2003), Moore et al. (2003), Wu et al. (2012, 2013), Palumbo et al. (2004), Brunetto et al., 2006), and have demonstrated the synthesis in the solid phase of a large number of C, H, O-bearing molecules, including hydrocarbons, nitriles, radicals, and anions, some of which may survive in the temperature regime of Pluto's surface. The Wu et al. (2012, 2013) experiments show that the same basic suite of molecules and radicals is formed from the same starting ice mix whether the energy source is UV or electrons. Wu et al. noted that some of the volatile products of their irradiation experiments might account for the absorption observed in the interval 210–240 nm in Pluto's UV spectrum observed by Stern et al. (2012). Bohn et al. (1994) emphasize the potential importance of the reactive molecule CH_2N_2 (diazomethane) that results from UV irradiation of ice mixtures of N_2 , CH_4 , and CO . These experiments were focused on the volatile irradiation products, and the more refractory complex residue was not collected for analysis. We consider the refractory residue question below.

Ultraviolet and electron irradiation of mixtures of ices found on Pluto (CH_4 , N_2 , CO , C_2H_6) produces a lightly yellow-colored residue that is stable at room temperature (Materese et al., 2014). This

residue contains carboxylic acids, aliphatic structures and HCN (probably as a polymer), but very little aromatic material. This refractory residue is potentially relevant to a large number of transneptunian objects that have ices of CH₄, N₂, and CO. The UV opacity of Pluto's tenuous atmosphere of CH₄ shields the surface from solar ultraviolet light, but electrons penetrate the atmosphere and interact with the surface ices. As noted above, numerous radicals and other molecular fragments are produced at the low temperature of the laboratory experiments, and probably persist to some degree at Pluto's surface temperature.

Chemically and structurally complex refractory residues from the irradiation of mixtures of gases and ices of planetary relevance have become familiar as tholins (e.g., Khare et al., 1984; Imanaka et al., 2004, 2012; Coll et al., 1999; Quirico et al., 2008), which have colors ranging from yellow to orange to brown. The colors and low reflectances of organic materials are controlled by unsaturated bonds created when energetic photons and charged particles break up molecules that then recombine and cross-link with some degree of polymerization. Further absorption of energy causes carbonization, which darkens the solid material and eventually gives it a black color. Moroz et al. (2004) have further explored the solid-state physics of ion irradiation of complex organic mixtures.

Tholins are readily made in gaseous mixtures of nitrogen and hydrocarbons by energy deposition from sparks, corona discharge, or cold-cathode discharge, but are much more difficult to produce by the irradiation of ices in quantities suitable for analysis. Consequently, there are relatively few published results for ice-phase refractory materials. The complex refractive indices of some tholins have been measured (e.g., Khare et al., 1984; Imanaka et al., 2004, 2012), and have become essential components in the radiative transfer modeling of the surfaces of many planetary bodies (e.g., Cruikshank et al., 1998; Olkin et al., 2007). The general applicability of tholins as coloring agents in planetary settings has been discussed by Cruikshank et al. (2005). Poulet et al. (2002) demonstrated that the choice of radiative transfer modeling technique (e.g., the Hapke or the Shkuratov formulation) has a strong effect on the amount of tholin required to add color to a planetary surface.

Tholins produced by energy deposition in gaseous mixtures of CH₄ and N₂ consist of yellow to brown material composed of amorphous and unstructured carbon, carbon nitrides, aromatic structures with varying degrees of order, and aliphatic structures in the form of small side chains and bridging units. Formation at low gas pressures (~10–30 Pa) tend to produce red–brown residues with large aromatic structures in greater abundance and with more incorporated nitrogen than formation at higher pressures (~70–160 Pa). The higher pressures yield a more yellow color with less nitrogen in the aromatic rings and more saturated aliphatic hydrocarbons (Imanaka et al., 2004). Further details on the composition and structure of tholins can be found in Quirico et al. (2008 and references therein). It should be noted, however, that while organic refractory materials produced in the laboratory are useful analogs to the color materials on planetary surfaces, the conditions under which they are made do not accurately reflect the energetic environment of Pluto or the other Solar System bodies on which colored materials occur.

Complex organic materials are not the only naturally occurring red-colored materials. Some minerals relevant to Solar System bodies are red in color, although less so than the tholins; scattering models incorporating mafic silicates (Mg-pyroxene) and phyllosilicates (serpentine) can reproduce the red colors of Trojan asteroids, for example (Cruikshank et al., 2001; Emery and Brown, 2003). Although the hemisphere-averaged geometric albedo of Pluto through the visible spectral range is some 20 times larger than that of Trojan asteroids, lightcurve modeling of Pluto indicates that some regions of the surface have much lower albedo, approaching

the average albedo of the Trojans (~0.03 at 0.56 μm). This fact raises the possibility that the lowest albedo regions on Pluto may be colored by the presence of grains of mafic minerals and phyllosilicates incorporated in the ice or isolated as a lag deposit on or near the surface of the ice.

The color of Pluto is very nearly constant at all rotational aspects, even though there is a ~30% brightness modulation with rotation. The color is also constant with seasonal changes in the sub-Earth latitude, as well as with the planet's heliocentric distance. This is to say that the color has been quite constant for some 50 years, with the notable exception of the abrupt change in 2002 discussed above. Because most of Pluto's light is reflected from the bright surface materials, low-albedo surface components cannot change the color very much, at least when averaged over an entire hemisphere, as observed from Earth.

Germane to the issue of Pluto's color, Grundy (2009) has proposed an alternative view to the genesis of red organics by irradiation or precipitation on the surface of an icy body. He shows that if micrometer and sub-μm presolar grains of complex organics preserved from the interstellar medium are incorporated in the ice, the gradual concentration toward the surface can impart red coloration to the body as the ice evaporates or is preferentially ejected in impacts.

In addition, Clark et al. (2008) has found that a brightness peak in the blue spectral region on many satellites of Saturn can be understood as Rayleigh scattering caused by nanometer-size particles on the surface ice known to exist on these bodies. The color is neutral if the particles are carbon, but are distinctly red if the particles are neutral or oxidized iron. Spectrophotometric data of sufficient quality to reveal a potential Rayleigh scattering peak on Pluto have not yet been obtained.

In the cases of Pluto (and Triton), where there is an exchange of material between the surface and atmosphere on seasonal or other timescales, neither the Clark nor the Grundy mechanisms would seem to be effective, and the surface exposures of red colored minerals may similarly be seen as unlikely. We are thus left with the likelihood that the *in situ* genesis of complex organic materials produced in the surface ices and in the atmosphere constitute the major non-ice component on Pluto. These materials are produced continuously because the supply of nitrogen, hydrocarbons, and energy is unending.

3. Charon

3.1. Ices detected on Charon: H₂O and hydrated NH₃

Charon was discovered in 1978, just a few years in advance of the epoch of mutual transits and occultations with the planet. Although at that time the planet and the satellite could not be resolved from one another for conventional spectroscopy of Charon alone, Buie et al. (1987) and Marcialis et al. (1987) used a subtractive technique during the mutual events to isolate the spectrum of Charon. The low-resolution spectrum in the wavelength interval 1.5–2.5 μm (13 spectral points in the Buie et al. work) clearly showed the absorption due to water ice at 1.55, 2.0, and 2.4 μm, but with no indication of methane ice, in contrast to Pluto.

Optical techniques improved and eventually enabled the first spectra that could resolve Charon's signal from that of Pluto. The first results confirmed the Buie et al. (1987) and Marcialis et al. (1987) results and better defined the H₂O–ice bands at 1.5, 1.65, and 2.0 μm (Brown and Calvin, 2000; Buie and Grundy, 2000; Dumas et al., 2001) that are globally distributed. Notably, the higher-resolution spectra obtained by these investigators clearly showed the 1.65-μm ice band indicative of crystalline H₂O, although at the low temperature of Charon ($T \leq 50$ K) the

amorphous phase was expected. An additional band at 2.21 μm was attributed to ammonia hydrates ($\text{NH}_3 \cdot n\text{H}_2\text{O}$; Brown and Calvin, 2000; Buie and Grundy, 2000; Dumas et al., 2001; Verbiscer et al., 2007). Merlin et al. (2010) tentatively detected the ammonia hydrate absorption feature at 2.0 μm .

H_2O -ice can exist in three phases: amorphous, cubic crystalline, or hexagonal crystalline (Cruikshank et al., 1998; Jenniskens et al., 1998; Schmitt et al., 1998). Amorphous ice has three broad features in the near-infrared at 1.5, 1.56 (that blend together to form one wide band) and at 2.0 μm . Crystalline ice is distinguished by an additional feature at 1.65 μm . While the near-infrared bands are the easiest to measure on the surfaces of outer Solar System bodies, they are in fact the intrinsically weakest ice bands as they are overtones and combinations of vibrations at longer wavelengths (Gerakines et al., 2005; Hudgins et al., 1993; Ockman, 1958).

It is, in fact, quite astonishing that with very few exceptions all of the solid bodies in the Solar System beyond Mars where H_2O ice has been detected spectroscopically show the presence of the crystalline phase, although the prevalent low temperatures ($T < 135$ K) and the expected (lower) temperatures of condensation indicate that the amorphous phase should be dominant. The widespread occurrence of crystalline H_2O ice on very cold bodies in the outer Solar System remains to be explained.

Mastrapa and Brown (2006) showed that ion irradiation of crystalline ice produces defects at the molecular level, changing the diagnostic spectral features to give the appearance of amorphous ice without actually changing the bulk structure. Mastrapa et al. (2006) further explored the temperature and radiation effects on amorphous and crystalline H_2O -ice and found that the near-infrared features of crystalline H_2O -ice are strongly temperature dependent, in accord with the extensive study of the crystalline (hexagonal) bands by Grundy and Schmitt (1998). In particular, the 1.65- μm feature becomes weaker when heated and grows stronger when cooled, and the 2- μm band shifts to shorter wavelengths with higher temperature. Amorphous ice displays spectral changes when deposited above or below 70 K, but otherwise no clear changes with temperature were seen in the Mastrapa et al. (2008) study. The amorphous and crystalline phases are spectrally indistinguishable at 170 K (Mastrapa et al., 2006).

In the mid-infrared, absorption bands are also dependent on deposition temperature, and the changes are most prominent for the 3- μm band. For crystalline ice, there are three bands at 3.0, 3.1 and 3.2 μm that make up the absorption feature, while for amorphous ice there is a single feature centered at 3.1 μm . Mastrapa et al. (2009) find that at 3 μm , the amorphous band and the 3.1- and 3.2- μm bands of crystalline ice gradually grow stronger and shifts to longer wavelength when deposited at higher temperatures. Clark et al. (2012) noticed important differences between their laboratory spectra and spectrum models calculated with the Mastrapa et al. (2009) optical constants over the 3.2–5.0 μm range and at the same temperature. Clark et al. (2012) modified the constants in this region to obtain a better fit to the laboratory data, and used the modified constants in a study of the spectra of several satellites of Saturn.

Amorphization of crystalline H_2O -ice by irradiation is also temperature dependent. At low temperatures (<50 K) the irradiated crystalline spectrum looks similar to amorphous ice, but at higher temperatures (>50 K) the crystalline feature at 1.65 μm is still present (Moore and Hudson, 1992; Strazzulla et al., 1992; Mastrapa et al., 2006).

In the first L band (3.0–4.1 μm) observations of Charon, Protopapa et al. (2008) detected a broad H_2O ice signature. They found that the standard model from Buie and Grundy (2000) consisting of an intimate mixture of 60% H_2O ice with 40% of a neutral continuum absorber adequately matches their spectrum out to

4 μm , except that the component must absorb less beyond 3.2 μm than predicted in the standard model.

Krasnopolsky (2001a,b) presented the first ultraviolet spectra of Charon from Hubble Space Telescope data in the range 225–330 nm, finding that the geometric albedo across this range is very nearly constant at 0.23. He searched for ultraviolet absorption bands of CO_2 , NH_3 , and SO_2 ices, but found none, noting that the upper limits for these molecules are high and nonrestrictive. Neither were UV bands of H_2O ice detected in this spectral region, although the presence of H_2O is well established.

3.2. Nature and distribution of NH_3

The 2.21- μm absorption band seen on Charon was the first detection of ammonia hydrate in the Solar System; its occurrence had been predicted by Croft et al. (1988) and Kargel (1992). In spectra of two opposite hemispheres of Charon (the Pluto-facing and the anti-Pluto sides) Cook et al. (2007) found a shift of 0.014 μm in the 2.21- μm band position. They suggested that different degrees of hydration of the NH_3 could account for the wavelength difference. A follow-up study with greater surface coverage finds, instead, only weak variation in the position of the 2.21- μm band across the surface that could be due to varying concentrations of NH_3 diluted in H_2O (DeMeo et al., this issue). The depth of the ammonia hydrate band displays weak spatial variation. Fig. 5 from Merlin et al. (2010) shows the spectrum of Charon with the H_2O ice and ammonia features indicated.

The presence of ammonia hydrate on Charon's surface is surprising because it should be quickly destroyed from irradiation by ultraviolet light and charged particles (Strazzulla and Palumbo, 1998; Cooper et al., 2003). Cook et al. (2007) investigated the likelihood of a variety of mechanisms to maintain or resupply ammonia hydrate on the surface including cryovolcanism, impact gardening, and solid-state greenhouse or convection. They favored cryovolcanism as the most plausible scenario, but the possibility of the diffusion of NH_3 from the interior into the surface H_2O ice, where it will undergo a hydration reaction, should be investigated.

3.3. Non-ice component of Charon's surface

Globally, Charon's albedo is significantly lower than that of Pluto, and its color on the sub-Pluto hemisphere is nearly a neutral gray, with the Binzel (1988) value of $B-V = 0.700 \pm 0.010$ ($(B-V)_{\text{Sun}} = 0.65$). A more recent globally constant value of $(B-V) = 0.7315 \pm 0.0013$ was determined by Buie et al. (2010a). The slight difference between these values can be attributed to the wavelength dependence of Charon's phase curve (Buie et al., 2010a). At the photometric B band (0.44 μm), Tholen and Buie (1990) give the geometric albedo of Pluto as 0.44–0.61, and that for Charon 0.38. The near-infrared spectrum is more blue toward longer wavelengths than would be expected for a mixture of crystalline water ice and ammonia hydrate, and neither pure H_2O ice nor NH_3 hydrate have low albedos. Another neutrally absorbing component in the spectrum, perhaps similar to that seen on other icy satellites (Buie and Grundy, 2000), is clearly indicated. Merlin et al. (2010) suggest that the presence of an amorphous water ice component of the surface could contribute to this blue spectral trend, but in the end favor the presence of another surface constituent in addition to the H_2O and NH_3 hydrate(s).

4. Comparison with other outer Solar System bodies

Pluto has a handful of fellow members of the Kuiper Belt of comparable size and composition. Pluto's near twin is the trans-neptunian object Eris. At 1163 ± 6 km across (Sicardy et al.,

2011), Eris is essentially the same size as Pluto, although its temperature is lower throughout most of its orbit since it has a semi-major axis of 67 AU, while Pluto's semimajor axis is 39 AU. Eris has no appreciable lightcurve, but its surface composition is strikingly similar to that of Pluto, with a surface dominated by solid nitrogen and smaller amounts of solid methane attributed to a pure component and one diluted in the nitrogen (Brown et al., 2005; Licandro et al., 2006a; Dumas et al., 2007; Merlin et al., 2007, 2009; Tegler et al., 2010; Alvarez-Candal et al., 2011). In contrast to Pluto, on Eris we cannot directly detect the presence of nitrogen because at the low temperatures expected on the surface, nitrogen should be in the α -phase, which has much narrower spectral bands than the β -phase. Instead, shifts in the methane absorption bands indirectly indicate dilution in nitrogen.

The transneptunian object Makemake is also methane-rich. In fact, its surface is expected to be covered with essentially pure slabs of methane because the absorption bands are saturated (Licandro et al., 2006b; Brown et al., 2007a). Ethane is also seen on Makemake's surface, clearly visible as an expected irradiation product of the methane (Brown et al., 2007a, 2007b). Other TNOs with methane are Sedna and Quaoar, but their spectra are not dominated by methane features (Barucci et al., 2005; Schaller and Brown, 2007b).

Concerning the issue of pure methane ice, we refer the reader back to Section 2.1 of this paper.

Charon, with a radius of 604 km (Sicardy et al., 2006), is comparable to the mid-sized TNOs and the four largest uranian satellites, and at the level of our understanding does not exhibit unique characteristics. The occurrence of the crystalline phase of water ice is widespread in the Kuiper Belt (Barkume et al., 2008; Guilbert et al., 2009). The mid-size objects that have diameters around 1000 km and greater are bright enough to yield spectra of sufficient quality to detect the characteristic 1.65- μm band of crystalline H_2O , seen on Haumea (Trujillo et al., 2007), Orcus (de Bergh et al., 2005), and Quaoar (Jewitt and Luu, 2004). Haumea is large enough that we would expect it to retain ices more volatile than water, such as methane or ammonia, and their absence is suspected to be due to the major collision that created the Haumea family (Brown et al., 2007b). Quaoar resides in a transition region for volatile retention (Schaller and Brown, 2007a), and a few weak absorption features indicate the presence of some methane and ethane (Schaller and Brown, 2007b). Orcus could be considered Charon's closest twin as it has strong crystalline ice absorption, and also a distinct 2.21- μm absorption band that is attributed to ammonia hydrate (de Bergh et al., 2004; Barucci et al., 2008).

New Horizons will give a close-up view of Charon's geology and its possible spectral variegation, and will provide a sensitive test for the presence of an atmosphere. The *New Horizons* investigation may reveal unique characteristics of Charon, possibly related to its proximity to Pluto, but at the very least it will provide an important baseline for the interpretation of the physical properties of other outer Solar System bodies and overall similar surface and bulk compositions.

Many of the icy satellites of the giant planets have strong crystalline H_2O ice bands that resemble those of Charon (e.g., Calvin et al., 1995; Grundy et al., 1999; Filacchione et al., 2012). The most similar are the regular uranian satellites Oberon, Titania, Umbriel and Ariel, although none have the 2.21- μm band of ammonia hydrate, and all but Oberon have measurable amounts of CO_2 on their surfaces (Grundy et al., 2006).

5. Conclusions

Advances in detection technology, powerful spectrometers, space-based facilities, and the advent of very large ground-based

telescopes have enabled great progress in unveiling Pluto and its system of satellites since the earliest diagnostic observations in the late-1970s. Adaptive optical techniques with the largest telescopes facilitate the spectroscopic study of Pluto and Charon separately, enabling detailed study of distinctly different compositions on these two bodies. Both Pluto and Charon show surface inhomogeneity in the distribution of their respective ices, and subtle but clear secular changes in the infrared spectrum of Pluto have been detected. These effects and their understanding are at the frontier of current studies of the Pluto–Charon system, and by implication, the numerous similar bodies that compose the Kuiper Belt and indeed the entire transneptunian object population. At the same time, laboratory studies of ices of H_2O , N_2 , CH_4 , C_2H_6 , CO , and other species over a range of temperatures and structural phases have provided a firm basis for the detection and identification of the principal neutral components of the solid surfaces of both Pluto and Charon, as well as the larger transneptunian population. Radiative transfer modeling using the complex refractive indices derived for the known ices have given insight into the way the ices are mixed, both vertically in the uppermost surface layers and geographically on a large scale.

The nature of the coloring material on both Pluto and Charon remains to be clarified through additional astronomical and spacecraft observations, supported by laboratory measurements of the effects of the space environment on the ices already identified. It has been clearly shown that complex radiation chemistry occurs at Pluto temperatures when the known ice components are exposed to ultraviolet light and to charged particles, but the exact pathways from ices to colored material are not yet understood. *New Horizons* will not only reveal the surfaces of Pluto and Charon in unprecedented geographic and spectroscopic detail, and together with corresponding data on the atmosphere, will stimulate new laboratory studies and modeling efforts. The knowledge of the Pluto–Charon system gained through the *New Horizons* investigation will quickly propagate to further elucidate the physical properties of the vast number of varied icy bodies in the outer Solar System. That new insight will, in turn, bring new understanding of the corresponding bodies in the many planetary systems currently being discovered in neighboring regions of the Milky Way, and by extension, throughout the Galaxy.

References

- Abernathy, M.R., Tegler, S.C., Grundy, W.M., et al., 2009. Digging into the surface of the icy dwarf planet Eris. *Icarus* 199, 520–525.
- Alvarez-Candal, A., Pinilla-Alonso, N., Licandro, J., et al., 2011. The spectrum of (136199) Eris between 350 and 2350 nm: Results with X-Shooter. *Astron. Astrophys.* 523, A130, 8 pages.
- Barker, E.S., Cochran, W.D., Cochran, A.L., 1980. Spectrophotometry of Pluto from 3500 to 7350 Å. *Icarus* 44, 43–52.
- Barkume, K.M., Brown, M.E., Schaller, E.L., 2008. Near-infrared spectra of centaurs and Kuiper Belt objects. *Astron. J.* 135, 55–67.
- Barucci, M.A., Cruikshank, D.P., Dotto, E., et al., 2005. Is Sedna another Triton? *Astron. Astrophys.* 439, L1–L4.
- Barucci, M.A., Merlin, F., Guilbert, A., et al., 2008. Surface composition and temperature of the TNO Orcus. *Astron. Astrophys.* 479, L13–L16.
- Bell, J.F., Clark, R.N., McCord, T.B., Cruikshank, D.P., 1979. Reflection spectra of Pluto and three distant satellites. *Bull. Am. Astron. Soc.* 11, 570 (Abstract).
- Binzel, R.P., 1988. Hemispherical color differences on Pluto and Charon. *Science* 241, 1070–1072.
- Bohn, R.B., Sandford, S.A., Allamandola, L.J., Cruikshank, D.P., 1994. Infrared spectroscopy of Triton and Pluto ice analogs: The case for saturated hydrocarbons. *Icarus* 111, 151–173.
- Brown, M.E., Calvin, W.M., 2000. Evidence for crystalline water and ammonia ices on Pluto's satellite Charon. *Science* 287, 107–109.
- Brown, M.E., Trujillo, C.A., Rabinowitz, D.L., 2005. Discovery of a planetary-sized object in the scattered Kuiper Belt. *Astrophys. J.* 635, L97–L100.
- Brown, M.E., Barkume, K.M., Blake, G.A., et al., 2007a. Methane and ethane on the bright Kuiper Belt object 2005 FY9. *Astron. J.* 133, 284–289.
- Brown, M.E., Barkume, K.M., Ragozzine, D., Schaller, E.L., 2007b. A collisional family of icy objects in the Kuiper belt. *Nature* 446, 294–296.

- Brunetto, R., Barucci, M.A., Dotto, E., Strazzulla, G., 2006. Ion irradiation of frozen methanol, methane, and benzene: Linking to the colors of centaurs and TNOs. *Astrophys. J.* 644, 646–650.
- Brunetto, R., Caniglia, G., Baratta, G.A., Palumbo, M.E., 2008. Integrated near-infrared band strengths of solid CH₄ and its mixtures with N₂. *Astrophys. J.* 686, 1480–1485.
- Buie, M.W., Fink, U., 1987. Methane absorption variations in the spectrum of Pluto. *Icarus* 70, 483–498.
- Buie, M.W., Grundy, W.M., 2000. The distribution and physical state of H₂O on Charon. *Icarus* 148, 324–339.
- Buie, M.W., Cruikshank, D.P., Lebofsky, L.A., Tedesco, E.F., 1987. Water frost on Charon. *Nature* 329, 522–523.
- Buie, M.W., Tholen, D.J., Horne, K., 1992. Albedo maps of Pluto and Charon: Initial mutual event results. *Icarus* 97, 211–227.
- Buie, M.W., Young, E.F., Binzel, R.P., 1997. Surface appearance of Pluto and Charon. In: Stern, S.A., Tholen, D.J. (Eds.), *Pluto and Charon*. Univ. Arizona Press, Tucson, pp. 269–293.
- Buie, M.W., Grundy, W.M., Young, E.F., Young, L.A., Stern, S.A., 2010a. Pluto and Charon with the Hubble Space Telescope II. Monitoring global change and improved surface properties from light curves. *Astron. J.* 139, 1117–1127.
- Buie, M.W., Grundy, W.M., Young, E.F., Young, L.A., Stern, S.A., 2010b. Pluto and Charon with the Hubble Space Telescope II. Resolving changes on Pluto's surface and a map for Charon. *Astron. J.* 139, 1128–1143.
- Buie, M.W., Tholen, D.J., Grundy, W.M., 2012. The orbit of Charon is circular. *Astron. J.* 144 (1), 19pp. Article ID 15.
- Burgdorf, M.J., Cruikshank, D.P., Dalle Ore, C.M., 2010. A tentative identification of HCN ice on Triton. *Astrophys. J.* 718, L53–L57.
- Calvin, W.M., Clark, R.N., Brown, R.H., Spencer, J.R., 1995. Spectra of the icy Galilean satellites from 0.2 to 5 microns: A compilation, new observations, and a recent summary. *J. Geophys. Res.* 100, 19041–19048.
- Clark, R.N., Brown, R.H., Jaumann, R., et al., 2008. Compositional mapping of Saturn's satellite Dione with Cassini VIMS and the implications of dark material in the Saturn system. *Icarus* 193, 372–386.
- Clark, R.N., Cruikshank, D.P., Jaumann, R., et al., 2012. The surface composition of Iapetus: Mapping results from Cassini VIMS. *Icarus* 218, 831–860.
- Coll, P., Coscia, D., Smith, N., et al., 1999. Experimental laboratory simulation of Titan's atmosphere: Aerosols and gas phase. *Planet. Space Sci.* 47, 1331–1340.
- Cook, J.C., Desch, S.J., Roush, T.L., Trujillo, C.A., Geballe, T.R., 2007. Near-infrared spectroscopy of Charon: Possible evidence for cryovolcanism on Kuiper Belt objects. *Astrophys. J.* 663, 1406–1419.
- Cook, J.C., Cruikshank, D.P., Young, L.A., 2013. Observations of Pluto's surface and atmosphere at low resolution. Paper Presented at Pluto Conference, Applied Physics Lab., July 22–26.
- Cooper, J.F., Christian, E.R., Richardson, J.D., Wang, C., 2003. Proton irradiation of Centaur, Kuiper Belt, and Oort cloud objects at plasma to cosmic ray energy. *Earth Moon Planet.* 92, 261–277.
- Croft, S.K., Lunine, J.I., Kargel, J., 1988. Equation of state of ammonia–water liquid: Derivation and planetological applications. *Icarus* 73, 279–293.
- Cruikshank, D.P., Silvggio, P.M., 1980. The surface and atmosphere of Pluto. *Icarus* 41, 96–102.
- Cruikshank, D.P., Pilcher, C.B., Morrison, D., 1976. Pluto: Evidence for methane ice. *Science* 194, 835–837.
- Cruikshank, D.P., Brown, R.H., Clark, R.M., 1984. Nitrogen on Triton. *Icarus* 58, 293–305.
- Cruikshank, D.P., Brown, R.H., Tokunaga, A.T., et al., 1988. Volatiles on Triton: The infrared spectral evidence, 2.0–2.5 micrometers. *Icarus* 74, 413–423.
- Cruikshank, D.P., Roush, T.L., Owen, T.C., et al., 1993. Ices on the surface of Triton. *Science* 261, 742–745.
- Cruikshank, D.P., Roush, T.L., Moore, J.M., et al., 1997. The surfaces of Pluto and Charon. In: Stern, S.A., Tholen, D.J. (Eds.), *Pluto and Charon*. Univ. Arizona Press, Tucson, pp. 221–267.
- Cruikshank, D.P., Dalle Ore, C.M., Roush, T.L., 2001. Constraints on the composition of Trojan Asteroid 624 Hektor. *Icarus* 153, 348–360.
- Cruikshank, D.P., Imanaka, H., Dalle Ore, C.M., 2005. Tholins as coloring agents on outer Solar System bodies. *Adv. Space Res.* 36, 178–183.
- Cruikshank, D.P., Mason, R.E., Dalle Ore, C.M., et al., 2006. Ethane on Pluto and Triton. *Bull. Am. Astron. Soc.* 38, 518 (Abstract).
- Cruikshank, D.P., Roush, T.L., Bartholomew, M.J., et al., 1998. The composition of centaur 5145 Pholus. *Icarus* 135, 389–407.
- de Bergh, C., Delsanti, A., Tozzi, G.-P., et al., 2004. The surface of transneptunian object 2004 DW. *Bull. A.A.S.* 36, 1102 (Abstract).
- de Bergh, C., Delsanti, A., Tozzi, G.P., et al., 2005. The surface of the transneptunian object 90482 Orcus. *Astron. Astrophys.* 437, 1115–1120.
- DeMeo, F.E., Dumas, C., de Bergh, C., et al., 2010. A search for ethane on Pluto and Triton. *Icarus* 208, 412–424.
- Douté, S., Schmitt, B., Quirico, E., et al., 1999. Evidence for methane segregation at the surface of Pluto. *Icarus* 142, 421–444.
- Dumas, C., Terrile, R.J., Brown, R.H., Schneider, G., Smith, B.A., 2001. Hubble Space Telescope NICMOS Spectroscopy of Charon's leading and trailing hemispheres. *Astron. J.* 121, 1163–1170.
- Dumas, C., Merlin, F., Barucci, M.A., et al., 2007. Surface composition of the largest dwarf planet 136199 Eris 2003 UB₃₁₃. *Astron. Astrophys.* 421, 331–334.
- Elliot, J.L., Ates, A., Babcock, B.A., et al., 2003. The recent expansion of Pluto's atmosphere. *Nature* 424, 165–168.
- Emery, J.P., Brown, R.H., 2003. Constraints on the surface composition of Trojan asteroids from near-infrared (0.8–4.0 μm) spectroscopy. *Icarus* 164, 104–121.
- Filacchione, G., Capaccioni, F., Ciarniello, M., et al., 2012. Saturn's icy satellites and rings investigated by Cassini–VIMS: III – Radial compositional variability. *Icarus* 220, 1064–1096.
- Fink, U., DiSanti, M.A., 1988. The separate spectra of Pluto and its satellite Charon. *Astron. J.* 95, 229–236.
- Fray, N., Schmitt, B., 2009. Sublimation of ices of astrophysical interest: A bibliographic review. *Planet. Space Sci.* 57, 2053–2080.
- Gerakines, P.A., Bray, J.J., Davis, A., Richey, C.R., 2005. The strengths of near-infrared absorption features relevant to interstellar and planetary ices. *Astrophys. J.* 620, 1140–1150.
- Grundy, W.M., 2009. Is the missing ultra-red material colorless ice? *Icarus* 199, 560–563.
- Grundy, W.M., Buie, M.W., 2001. Distribution and evolution of CH₄, N₂, and CO ices on Pluto's surface: 1995 to 1998. *Icarus* 153, 248–263.
- Grundy, W.M., Fink, U., 1996. Synoptic CCD spectrophotometry of Pluto over the past 15 years. *Icarus* 124, 329–343.
- Grundy, W.M., Schmitt, B., 1998. The temperature-dependent near-infrared absorption spectrum of hexagonal H₂O ice. *J. Geophys. Res. (E)* 103, 25809–25822.
- Grundy, W.M., Schmitt, B., Quirico, E., 1993. The temperature dependent spectra of alpha and beta nitrogen ice with application to Triton. *Icarus* 105, 254–258.
- Grundy, W.M., Buie, M.W., Stansberry, J.A., Spencer, J.R., Schmitt, B., 1999. Near-infrared spectra of icy outer Solar System surfaces: Remote determination of H₂O ice temperatures. *Icarus* 142, 536–549.
- Grundy, W.M., Schmitt, B., Quirico, E., 2002. The temperature-dependent spectrum of methane ice I between 0.7 and 5 microns and opportunities for near-infrared remote thermometry. *Icarus* 155, 486–496.
- Grundy, W.M., Young, L.A., Spencer, J.R., et al., 2006. Distributions of H₂O and CO₂ ices on Ariel, Umbriel, Titania, and Oberon from IRTF/SpEx observations. *Icarus* 184, 543–555.
- Grundy, W.M., Olkin, C.B., Young, L.A., Buie, M.W., Young, E.F., 2013. Near-infrared spectral monitoring of Pluto's ices: Spatial distribution and secular evolution. *Icarus* 223, 710–721.
- Grundy, W.M., Olkin, C.B., Young, L.A., Holler, B.J., 2014. Near-infrared spectral monitoring of Pluto's ices II: Recent decline of CO and N₂ ice absorptions. *Icarus* 235, 220–224.
- Guilbert, A., Alvarez-Candal, A., Merlin, F., et al., 2009. ESO-large program on TNOs: Near-infrared spectroscopy with SINFONI. *Icarus* 201, 272–283.
- Hudgins, D., Sandford, S.A., Allamandola, L.J., Tielens, A.G.G.M., 1993. Mid- and far infrared spectroscopy of ices: Optical constants and integrated absorbances. *Astrophys. J. Suppl. Ser.* 86, 713–870.
- Imanaka, H., Khare, B.N., Elsila, J.E., et al., 2004. Laboratory experiments of Titan tholin formed in cold plasma at various pressures: Implications for nitrogen-containing polycyclic aromatic compounds in Titan haze. *Icarus* 168, 344–366.
- Imanaka, H., Cruikshank, D.P., Khare, B.N., McKay, C.P., 2012. Optical constants of laboratory synthesized complex organic materials: Part 1. Titan tholins at mid-infrared wavelengths (2.5–25 μm). *Icarus* 218, 247–261.
- Jenniskens, P., Blake, D.F., Kouchi, A., 1998. Amorphous water ice: A Solar System material. In: Schmitt, B., de Bergh, C., Festou, M. (Eds.), *Solar System Ices*. Kluwer, Dordrecht, pp. 139–155.
- Jewitt, D.C., Luu, J., 2004. Crystalline water ice on the Kuiper belt object (50000) Quaoar. *Nature* 432, 731–733.
- Kargel, J.S., 1992. Ammonia–water volcanism on icy satellites: Phase relations at 1 atmosphere. *Icarus* 100, 556–574.
- Khare, B.N., Sagan, C., Arakawa, E.T., et al., 1984. Optical constants of organic tholins produced in a simulated Titanian atmosphere: From soft X-ray to microwave frequencies. *Icarus* 60, 127–137.
- Krasnopolsky, V.A., 2001a. Middle ultraviolet spectroscopy of Pluto and Charon. *American Geophysical Union (Spring)*. Abstract #P22B-06.
- Krasnopolsky, V.A., 2001b. Middle ultraviolet spectroscopy of Pluto and Charon. *Icarus* 153, 277–284.
- Krasnopolsky, V.A., Cruikshank, D.P., 1999. Photochemistry of Pluto's atmosphere and ionosphere near perihelion. *J. Geophys. Res.* 104, 21979–21996.
- Lellouch, E., de Bergh, C., Sicardy, B., Kaufli, H.U., Smette, A., 2011a. High resolution spectroscopy of Pluto's atmosphere: Detection of the 2.3-μm CH₄ bands and evidence for carbon monoxide. *Astron. Astrophys.* 530, 4pp. Article ID L4.
- Lellouch, E., de Bergh, C., Sicardy, B., Kaufli, H.U., Smette, A., 2011b. The tenuous atmospheres of Pluto and Triton explored by CRILES on the VLT. *ESO Messenger* No. 145, pp. 20–23.
- Licandro, J., Grundy, W.M., Pinilla-Alonso, N., Leisy, P., 2006a. Visible spectroscopy of 2003 UB₃₁₃: Evidence for N₂ ice on the surface of the largest TNO? *Astron. Astrophys.* 458, L5–L8.
- Licandro, J., Pinilla-Alonso, N., Pedani, M., et al., 2006b. The methane ice rich surface of large TNO 2005 FY₉: A Pluto-twin in the trans-neptunian belt? *Astron. Astrophys.* 445, L35–L38.
- Lunine, J.I., Stevenson, D.J., 1985. Physical state of volatiles on the surface of Triton. *Nature* 317, 238–240.
- Madey, T.E., Johnson, R.E., Orlando, T.M., 2002. Far-out surface science: Radiation-induced surface processes in the Solar System. *Surf. Sci.* 500, 838–858.
- Marcialis, R.L., 1997. The first 50 years of Pluto–Charon research. In: Stern, S.A., Tholen, D.J. (Eds.), *Pluto and Charon*. Univ. Arizona Press, Tucson, pp. 27–83.
- Marcialis, R.L., Lebofsky, L.A., 1991. CVF spectrophotometry of Pluto: Correlation of composition with albedo. *Icarus* 89, 255–263.
- Marcialis, R.L., Rieke, G.H., Lebofsky, L.A., 1987. The surface composition of Charon: Tentative identification of water ice. *Science* 237, 1349–1351.

- Mastrapa, R.M., Brown, R.H., 2006. Ion irradiation of crystalline H₂O ice: Effect on the 1.65- μ m band. *Icarus* 183, 207–214.
- Mastrapa, R.M., Bernstein, M.P., Sandford, S.A., 2006. New optical constants for amorphous and crystalline H₂O-ice. American Geophysical Union. Abstract #P13C-0187.
- Mastrapa, R.M., Bernstein, M.P., Sandford, S.A., et al., 2008. Optical constants of amorphous and crystalline H₂O-ice in the near infrared from 1.1 to 2.6 μ m. *Icarus* 197, 307–320.
- Mastrapa, R.M., Sandford, S.A., Roush, T.L., et al., 2009. Optical constants of amorphous and crystalline H₂O ice: 2.5–22 μ m (4000–455 cm⁻¹). *Astrophys. J.* 701, 1347–1356.
- Materese, C.K., Cruikshank, D.P., Sandford, S.A., Imanaka, H., Nuevo, M., White, D., 2014. Ice chemistry on outer Solar System bodies: Carboxylic acids, nitriles, and urea detected in refractory residues produced from the UV-photolysis of N₂:CH₄:CO containing ices. *Astrophys. J.* 788, 11pp. Article ID 111.
- McKinnon, W.B., Simonelli, D.P., Schubert, G., 1997. Composition, internal structure, and thermal evolution of Pluto and Charon. In: Stern, S.A., Tholen, D.J. (Eds.), *Pluto and Charon*. Univ. Arizona Press, Tucson, pp. 295–343.
- Merlin, F., Guilbert, A., Dumas, C., et al., 2007. Properties of the icy surface of the TNO 136108 2003 EL₆₁. *Astron. Astrophys.* 466, 1185–1188.
- Merlin, F., Alvarez-Candal, A., Delsanti, A., et al., 2009. Stratification of methane ice on Eris' surface. *Astron. J.* 137, 315–328.
- Merlin, F., Barucci, M.A., de Bergh, C., et al., 2010. Chemical and physical properties of the variegated Pluto and Charon surfaces. *Icarus* 210, 930–943.
- Moore, M.H., Hudson, R.L., 1992. Far-infrared spectral studies of phase changes in water ice induced by proton irradiation. *Astrophys. J.* 401, 353–360.
- Moore, M.H., Hudson, R.L., 2003. Infrared study of ion-irradiated N₂-dominated ices relevant to Triton and Pluto: Formation of HCN and HNC. *Icarus* 161, 486–500.
- Moore, M.H., Hudson, R.L., Ferrante, R.F., 2003. Radiation products in processed ices relevant to Edgeworth–Kuiper-Belt objects. *Earth Moon Planets* 92, 291–306.
- Moroz, L.V., Baratta, G., Strazzulla, G., et al., 2004. Optical alteration of complex organics induced by ion irradiation: 1. Laboratory experiments suggest unusual space weathering trend. *Icarus* 170, 214–228.
- Nakamura, R., Sumikawa, S., Ishiguro, M., et al., 2000. Subaru infrared spectroscopy of the Pluto–Charon system. *Publ. Astron. Soc. Jpn.* 52, 551–556.
- Ockman, N., 1958. The infra-red and Raman spectra of ice. *Adv. Phys.* 7, 199–220.
- Olkin, C.B., Young, E.F., Young, L.A., et al., 2007. Pluto's spectrum from 1.0–4.2 μ m: Implications for surface properties. *Astron. J.* 133, 420–431.
- Olkin, C.B., Young, L.A., Borncamp, D., et al., 2014. Pluto's atmosphere does not collapse. *Icarus*, submitted for publication. <<http://arxiv.org/abs/1309.0841>>.
- Owen, T.C., Roush, T.L., Cruikshank, D.P., et al., 1993. Surface ices and atmospheric composition of Pluto. *Science* 261, 745–748.
- Palumbo, M.E., Ferini, G., Baratta, G.A., 2004. Infrared and Raman spectroscopies of refractory residues left over after ion irradiation of nitrogen-bearing icy mixtures. *Adv. Space Res.* 33, 49–56.
- Poulet, F., Cuzzi, J.N., Cruikshank, D.P., Roush, T., Dalle Ore, C.M., 2002. Comparison between the Shkuratov and Hapke scattering theories for solid planetary surfaces. Application to the surface composition of two centaurs. *Icarus* 160, 313–324.
- Prokhvatilov, A.I., Lantsevich, L.D., 1983. X-ray investigation of the equilibrium phase diagram of CH₄–N₂ solid mixtures. *Sov. J. Low Temp. Phys.* 9, 94–98.
- Protopapa, S., Boehnhardt, H., Herbst, 2008. Surface characterization of Pluto and Charon by L and M band spectra. *Astron. Astrophys.* 490, 365–375.
- Protopapa, S., Grundy, W.M., Tegler, S.C., et al., 2013. Absorption coefficients of the methane–nitrogen binary ice system: Implications for Pluto. *Bull. Amer. Astron. Soc.* 45 (No. 303.03).
- Quirico, E., Schmitt, B., 1997a. Near-infrared spectroscopy of simple hydrocarbons and carbon oxides diluted in solid N₂ and as pure ices: Implications for Triton and Pluto. *Icarus* 127, 354–378.
- Quirico, E., Schmitt, B., 1997b. A spectroscopic study of CO diluted in N₂ ice: Applications for Triton and Pluto. *Icarus* 128, 181–188.
- Quirico, E., Montagnac, G., Lees, V., et al., 2008. New experimental constraints on the composition and structure of tholins. *Icarus* 198, 218–231.
- Reinsch, K., Burwitz, V., Festou, M.C., 1994. Albedo maps of Pluto and improved physical parameters of the Pluto–Charon system. *Icarus* 108, 209–218.
- Sasaki, T., Kanno, A., Ishiguro, M., Kinoshita, D., Nakamura, R., et al., 2005. Search for nonmethane hydrocarbons on Pluto. *Astrophys. J.* 618, L57–L60.
- Schaefer, B.E., Buie, M.W., Smith, L.T., 2008. Pluto's light curve in 1933–1934. *Icarus* 197, 590–598.
- Schaller, E.L., Brown, M.E., 2007a. Volatile loss and retention on Kuiper Belt objects. *Astrophys. J.* 659, L61–L64.
- Schaller, E.L., Brown, M.E., 2007b. Detection of methane on Kuiper Belt object (50000) Quaoar. *Astrophys. J.* 670, L49–L51.
- Schmitt, B., de Bergh, C., Festou, M. (Eds.), 1998. *Solar System Ices*, vol. 227. Kluwer, Astrophys. Space Sci. Library, Dordrecht.
- Scott, T.A., 1976. Solid and liquid nitrogen. *Phys. Rep.* 27, 89–157.
- Sicardy, B., Widemann, T., Lellouch, E., et al., 2003. Large changes in Pluto's atmosphere as revealed by recent stellar occultations. *Nature* 424, 168–170.
- Sicardy, B., Bellucci, A., Gendron, E., et al., 2006. Charon's size and upper limit on its atmosphere from a stellar occultation. *Nature* 439, 52–54.
- Sicardy, B., Ortiz, J.L., Assafin, M., et al., 2011. A Pluto-like radius and a high albedo for the dwarf planet Eris from an occultation. *Nature* 478, 493–496.
- Soifer, B.T., Neugebauer, G., Matthews, K., 1980. The 1.5–2.5- μ m spectrum of Pluto. *Astron. J.* 85, 166–167.
- Spencer, J.R., Stansberry, J.A., Trafton, L.M., et al., 1997. Volatile transport, seasonal cycles, and atmospheric dynamics on Pluto. In: Stern, S.A., Tholen, D.J. (Eds.), *Pluto and Charon*. Univ. Arizona Press, Tucson, pp. 435–473.
- Stern, S.A., Buie, M.W., Trafton, L.M., 1997. HST high-resolution images and maps of Pluto. *Astron. J.* 113, 827–843.
- Stern, S.A., Cunningham, N.J., Hain, M.J., Spencer, J.R., Shinn, A., 2012. First ultraviolet reflectance spectra of Pluto and Charon by the Hubble Space Telescope Cosmic Origins Spectrograph: Absorption features and evidence for temporal change. *Astron. J.* 143 (1), 4pp. Article ID 22.
- Strazzulla, G., Palumbo, M.E., 1998. Evolution of icy surfaces: An experimental approach. *Planet. Space Sci.* 46, 1339–1348.
- Strazzulla, G., Baratta, G.A., Leto, G., Palumbo, M.E., 1992. Application of ion irradiation experiments to planetary surfaces in the outer solar system. *Earth Moon Planets* 56, 35–45.
- Tegler, S.C., Grundy, W.M., Vilas, F., et al., 2008. Evidence of N₂-ice on the surface of the icy dwarf planet 136472 (2005 FY₉). *Icarus* 195, 844–850.
- Tegler, S.C., Cornelison, D.M., Grundy, W.M., et al., 2010. Methane and nitrogen abundances on Pluto and Eris. *Astrophys. J.* 725, 1296–1305.
- Tegler, S.C., Grundy, W.M., Olkin, C.B., et al., 2012. Ice mineralogy across and into the surfaces of Pluto, Triton, and Eris. *Astrophys. J.* 751, 10pp. Article ID 76.
- Tholen, D.J., Buie, M.W., 1990. Further analysis of Pluto–Charon mutual event observations – 1990. *Bull. A.A.S.* 22, 1129 (Abstract).
- Tholen, D.J., Buie, M.W., 1988. Circumstances for Pluto–Charon mutual events in 1989. *Astron. J.* 96, 1977–1982.
- Trafton, L.M., Matson, D.L., Stansberry, J.A., 1998. Surface/atmosphere interactions and volatile transport (Triton, Pluto, and Io). In: Schmitt, B., de Bergh, C., Festou, M. (Eds.), *Solar System Ices*. Kluwer, Dordrecht, pp. 773–812.
- Trujillo, C.A., Brown, M.E., Barkume, K.M., Schaller, E.L., Rabinowitz, D.L., 2007. The surface of 2003 EL₆₁ in the near-infrared. *Astrophys. J.* 655, 1172–1178.
- Tryka, K.A., Brown, R.H., Anicich, V., Cruikshank, D.P., Owen, T.C., 1993. Spectroscopic determination of the phase composition and temperature of nitrogen ice on Triton. *Science* 261, 751–754.
- Tryka, K.A., Brown, R.H., Cruikshank, D.P., et al., 1994. Temperature of nitrogen ice on Pluto and its implications for flux measurements. *Icarus* 112, 513–527.
- Tryka, K.A., Brown, R.H., Anicich, V., 1995. Near-infrared absorption coefficients of solid nitrogen as a function of temperature. *Icarus* 116, 409–414.
- Verbiscer, A.J., Peterson, D.E., Skrutskie, M.F., et al., 2007. Simultaneous spatially-resolved near-infrared spectra of Pluto and Charon. In: *Lunar Planet. Sci.* vol. 38, p. 2318 (Abstracts).
- Wu, Y.J., Wu, C.Y.R., Chou, S.L., et al., 2012. Spectra and photolysis of pure nitrogen and methane dispersed in solid nitrogen with vacuum-ultraviolet light. *Astrophys. J.* 746, 11pp. Article ID 175.
- Wu, Y.J., Chen, H.F., Chuang, S.J., Huang, T.P., 2013. Ultraviolet and infrared spectra of electron-bombarded solid nitrogen and methane diluted in solid nitrogen. *Astrophys. J.* 768, 9pp. Article ID 83.